Available online at www.sciencedirect.com
SCIENCE DIRECT®
Journal of Luminescence 118 (2006) 220–226
JOURNAL OF LUMINESCENCE
www.elsevier.com/locate/jlumin

Dependence of photoluminescent properties of cubic $Y_2O_3:Tb^{3+}$ nanocrystals on particle size and temperature

Hongwei Song*, JiWei Wang

Key Laboratory of Excited State Physics, Changchun Institute of Optics, Fine Mechanics and Physics, Chinese Academy of Sciences, 16 Eastern Nan-Hu Road, Changchun 130033, P.R. China

Received 27 May 2005
Available online 3 October 2005

Abstract

Temperature-dependent spectral properties in the cubic $Y_2O_3:Tb^{3+}$ nanocrystals (NCs, 10–70 nm) under 488 nm excitation were studied and compared to that in the bulk. In NCs, emission lines assigned to the $^5D_4$–^7F_J ($J = 1-6$) transitions of Tb^{3+} ions and a broad band originated from oxygen defects were observed. As a function of temperature, two intensity maximums of the $^5D_4$–Σ^7F_J transitions appeared in the NCs, at ~250 and ~500 K, while in the bulk only one maximum appeared at ~250 K. The relative intensity of the maximum at ~500 K to that at ~250 K increased with decreasing particle size. The intensity maximum of the band emissions that came from the oxygen defects appeared in the range of 500–600 K. The appearance of intensity maximum as a function of temperature was attributed to the rivalry between thermal quenching process and phonon-assisted excitation. The appearance of two maxima in the NCs was attributed to the luminescence contributed by different Tb^{3+} centers, the internal and the surface. The emission for the surface Eu^{3+} centers has higher quenching temperature in contrast to that for the internal centers.

Keywords: Nanocrystals; Size-dependent luminescence; Thermal quenching

1. Introduction

The reduction of particle size of crystalline systems leads to important modification of some of their bulk properties due the following special electronic properties of nanometer particles: (1) the quantum size effect and (2) the increase of surface-to-volume ratio [1,2]. In 1994, Bhargava et al. [3] reported that Mn-doped nanocrystalline ZnS phosphors yielded very high luminescent quantum efficiency (QE). The electronic transition rate for Mn^{2+} in ZnS nanocrystals (NCs) was improved as high as five orders than that in the bulk materials. Despite this, the conclusion was seriously criticized later. The optical properties of nanocrystalline insulating semiconductor attracted

*Corresponding author. Tel./fax: +86 431 6176320.
E-mail addresses: songhw@ciomp.ac.cn, hwsong2005@yahoo.com.cn (H. Song).

0022-2313/$ - see front matter © 2005 Elsevier B.V. All rights reserved.
doi:10.1016/j.jlumin.2005.08.016

remarkable interest [4–6]. In recent years, rare earths (RE) -doped oxide nanocrystalline phosphors have also attracted considerable attention due to their potential application in lighting and display [7–10]. RE-doped yttria (Y_2O_3) are common phosphors in optical display and lighting applications, and the search for new phosphors has led to the preparation of nanocrystalline forms of Y_2O_3. Over the past several years, much attention has been given to them [11–15].

The luminescent properties of RE ions in NCs depend strongly on particle size and temperature. In previous papers, we systematically studied the temperature dependence of the fluorescence of cubic Y_2O_3:Eu^{3+} NCs prepared by combustion. We observed that the radiative and nonradiative transition rates for Eu^{3+} ions both increased with the decreasing particle size, due to crystal lattice degeneration and surface effect [16,17]. The charge transfer band for Eu^{3+} in nanocrystals was decreased by ultraviolet (UV) light irradiation due to surface effect [11,18]. In this paper, we demonstrate the interesting size and temperature dependencies of photoluminescent properties of Y_2O_3:Tb^{3+} NCs (7–70 nm) under 488 nm excitation in a wide temperature range (80–700 K), which is helpful of understanding the interaction between surface defects and luminescent centers.

2. Experiments

The Y_2O_3:Tb NCs were prepared by combustion method, which was originally reported by Tao et al. [19]. In the preparation, Y_2O_3 and Tb_4O_7 (in the molar ratio of 1: 0.01) were dissolved in nitric acid, and glycine was dissolved in distilled water; then the two kinds of solutions were mixed together to form the precursor. The solution was concentrated by heating until excess free water evaporated and spontaneous ignition occurred. The synthesis reaction function is

$$6\,M(NO_3)_3 + 10NH_2CH_2COOH + 18O_2 \rightarrow 3M_2O_3 + 5N_2 + 18NO_2 + 20CO_2 + 25H_2O.$$

After the combustion finished, the resultant Y_2O_3:Tb powders were formed. The particle size was controlled by adjusting the molar ratio of glycine to metal nitrate (G/N), which had affected the combustion temperature in the reaction. In the preparation, the values of G/N were controlled to be 1.00, 1.25, 1.45 and 1.67. To improve the crystallinity of the nanocrystalline powders and eliminate redundant nitrate, all the resultant Y_2O_3:Tb^{3+} were annealed at 500 °C for 2 h. In comparison, the bulk Y_2O_3:Tb powders were also prepared, by annealing the mixed Y_2O_3 and Tb_4O_7 powders (in the molar ratio of 1: 0.01) at 1200 °C for 6 h.

The crystal structure and particle size were obtained by X-ray diffraction (XRD) patterns, as shown in Fig. 1. As can be seen, all the NCs exhibited a pure cubic structure. The average crystalline size of the NCs was estimated by Scherrer formula to be ~7, 14, 35 and 70 nm, respectively, for the samples of $G/N = 1.00$, 1.25, 1.45 and 1.67. The sample of $G/N = 1.00$ was also characterized by transmission electron micrographs (TEM). The result demonstrated that the particles were nanospheres with an average size of ~5 nm, which was basically inconsistent with the calculated results by Scherrer formula [11]. Note

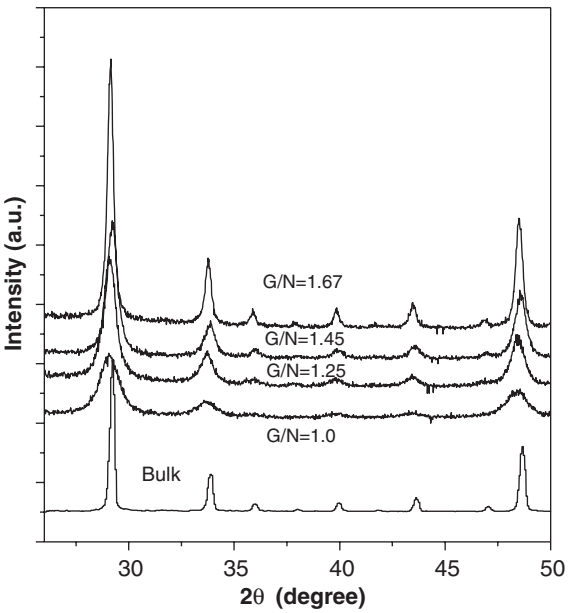

Fig. 1. XRD patterns of Y_2O_3:Tb^{3+} NCs prepared at different conditions.

that. as reported by the other authors, the particles tended to aggregate together. In the measurements of temperature-dependent luminescence, the samples were put into a liquid nitrogen cycling system (pellet), in which the temperature varied in the range of 80–700 K. A continuous 488 nm light that came from an argon laser was used as excitation source. The fluorescence was measured by a UV-Lab Raman Infinity (made by Jobin Yvon Company) with a resolution of $2\,cm^{-1}$.

3. Results and discussion

3.1. Dependence of photoluminescence on temperature and particle size

Fig. 2 shows photoluminescence spectra of different Y_2O_3 powders under 488 nm excitation (at 83 K). The sharp emission lines assigned to the $^5D_4$–^7F_J ($J = 1-6$) transitions of Tb^{3+} ions are discerned in the 35 nm, 70 nm and the bulk powders. Among them, the $^5D_4$–$^7F_5$ transitions are strongest. In the 7 and 14 nm powders, the $^5D_4$–^7F_J transitions for Tb^{3+} ions are relative weak and the emission lines become broader due to more disordered local environments surrounding Tb^{3+} ions. Besides the $^5D_4$–^7F_J lines, a broad emission band having a peak around 620 nm also appears, which should originate from the emissions of oxygen defects [20]. In the Er^{3+}- and Eu^{3+}-doped NCs, band emissions were also observed. Note that our Y_2O_3:Tb NCs contained some Tb^{4+} ions, which were identified by electron spin resonance (ESR) spectra [21]. Under the 266 nm ultraviolet laser irradiation, the valence state of Tb^{4+} did not change.

Fig. 3 shows the emission spectra measured at various temperatures in the 7 and 70 nm NCs. It can be seen that the emission intensities for both

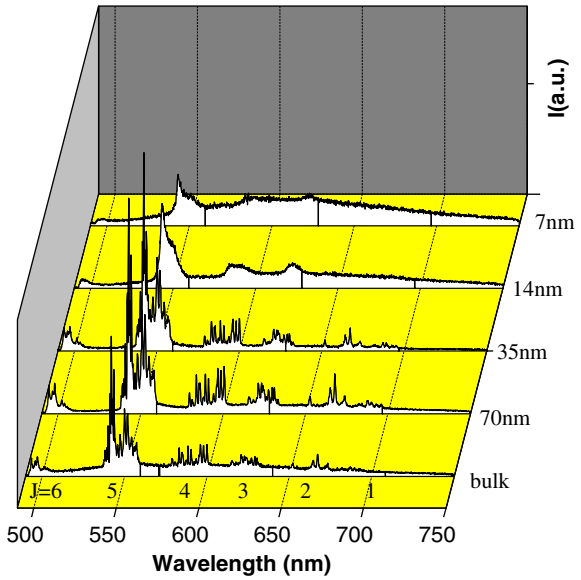

Fig. 2. Emission spectra of Y_2O_3:Tb^{3+} NCs under 488 nm laser excitation at 83 K.

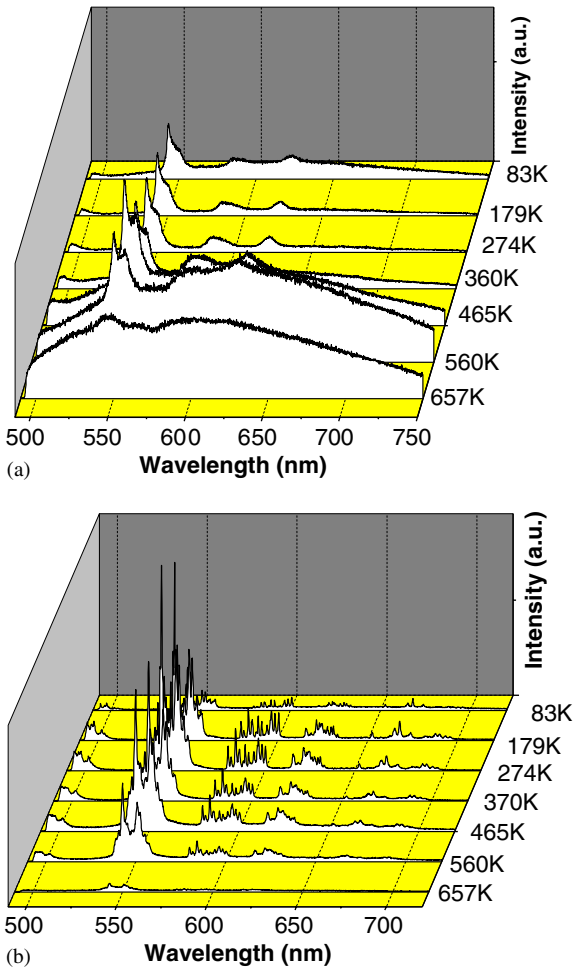

Fig. 3. Emission spectra of Y_2O_3:Tb^{3+} NCs at various temperatures in (a) the 7 nm NCs and (b) the 70 nm NCs.

$^5D_4$–^7F_J transitions and the broad band originated from oxygen defects and change remarkably with temperature. The emission intensity of the $^5D_4$–Σ^7F_J transitions as a function of temperature and of the broad band are shown in Figs. 4 and 5, respectively. As shown in Fig. 4, in NCs the emission intensity of the $^5D_4$–^7F_J transitions increases with elevated temperature originally and approaches a maximum around 250 K, then decreases in the range of 250–300 K. Above ~300 K, the emission intensity again increases with elevated temperature and approaches a maximum around 500 K, then decreases in the range of 500–700 K. The relative intensity of the maximum at ~250 and ~500 K varies greatly with particle size. The smaller the particle size, the lower the relative intensity of the maximum at ~250 K and the higher the relative intensity of the maximum at 500 K. In the bulk, there appears only one intensity maximum, at ~250 K. From Fig. 5 it can be seen that the emission intensity that originated from the oxygen defects decreases with increasing temperature below ~250 K, then increases with increasing temperature rapidly and approaches a maximum at a certain temperature and finally decreases with temperature. The intensity maximum for the 35 and 70 nm samples appears around 500 K, while that for the 7 and 14 nm samples appears around 600 K.

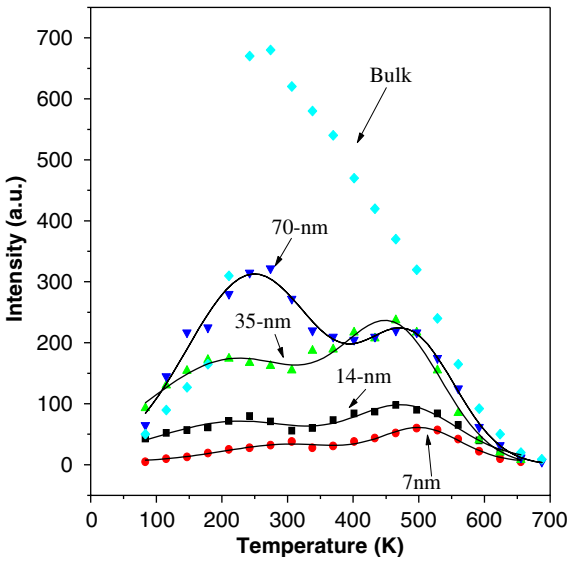

Fig. 4. Dependence of emission intensity of the $^5D_4$–$^7F_5$ transitions on temperature.

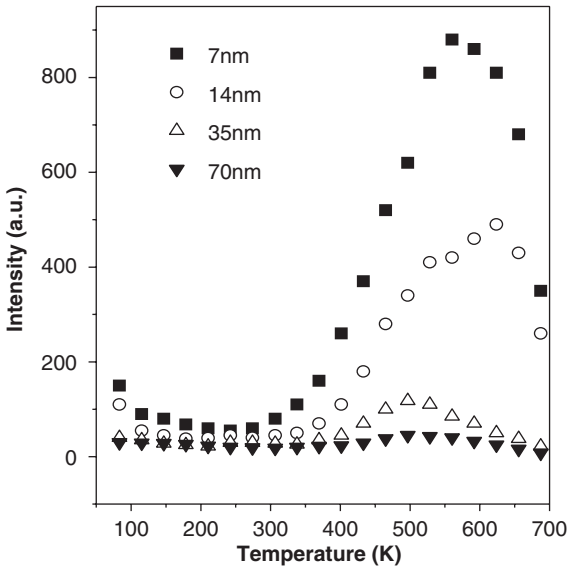

Fig. 5. Temperature dependence of emission intensity for the broad band originated from oxygen defects in various Y_2O_3:Tb^{3+} NCs.

From Figs. 4 and 5, it can also be seen that both the emission intensity of the $^5D_4$–^7F_J transitions and that of the broad band assigned to the oxygen vacancies vary with particle size. Fig. 6 gives the emission intensities of the $^5D_4$–^7F_J transitions and the broad band as a function of particle diameter. It is apparent that the emission intensity of the $^5D_4$–^7F_J transitions is proportional to the reverse of particle size, while that of the broad band assigned to the oxygen vacancies linearly increases with particle size. In NCs, a great number of surface defects are involved. Due to fast non-radiative energy transfer processes from the excited Tb^{3+} centers to the nearby surface defects, most Tb^{3+} centers locating in/near the surface become quenching centers, leading to the decrease of luminescent Tb^{3+} centers; thus, the total emission intensity of $^5D_4$–^7F_J transitions decreases with particle size, and the emissions from defect states increase. On the contrary, more oxygen defects are involved with decreasing particle size, leading to the increase of the band emissions.

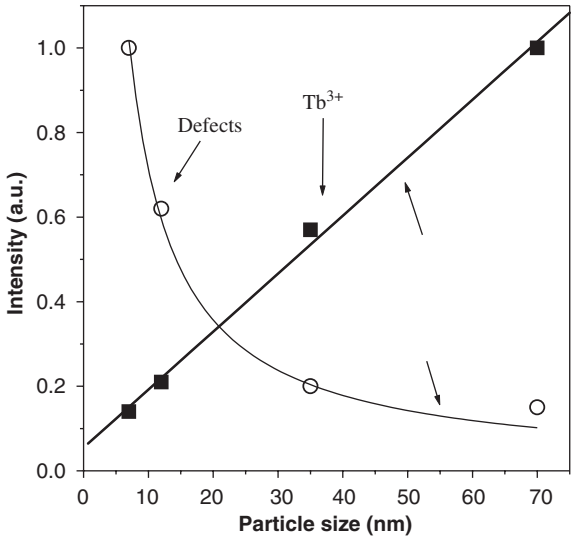

Fig. 6. Dependence of emission intensity of the $^5D_4$–^7F_J transitions for Tb^{3+} and the emission band originated from oxygen defects on particle diameter. The dots are experimental data and lines are fitting functions: $I_1 = 7.1/d$ for Tb^{3+} and $I_2 = 0.05 + 0.14d$ for oxygen defects.

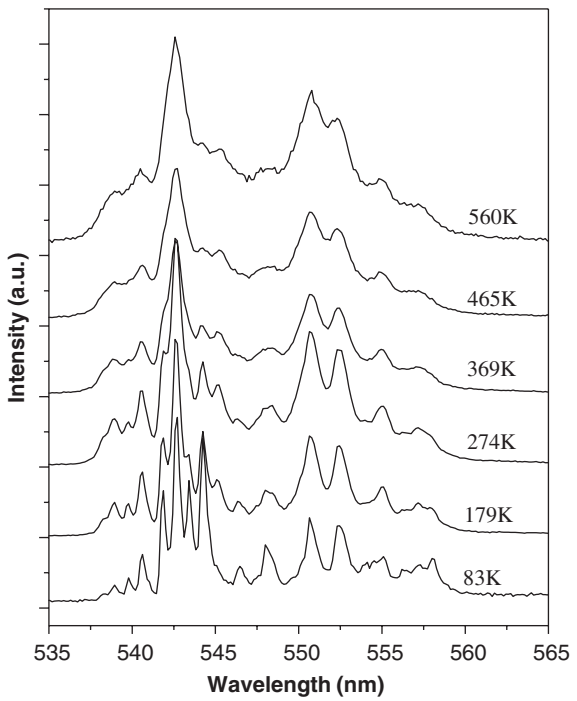

Fig. 7. Temperature dependence of the configuration of the $^5D_4$–$^7F_5$ emission lines in the 70 nm Y_2O_3:Tb^{3+} NCs.

As the temperature varies, the configuration of the $^5D_4$–^7F_J emission lines also changes. Fig. 7 shows the $^5D_4$–$^7F_5$ emission lines at various temperatures. At 83 K, a large number of Stark-splitting lines are distinguished. With elevated temperature, the full line widths of the Stark lines increase inhomogeneously/homogeneously and become broader. In addition, the relative intensity of different Stark lines also changes. For example, the relative intensity of the peak at ~544.0 nm to that at ~542.5 nm gradually decreases with elevated temperature. This can be attributed to the thermal redistribution of excited electrons on different Stark splitting levels of $^5D_4$.

3.2. Origin of temperature-dependent emission intensity

The 488 nm photon (20,491 cm^{-1}) is not exactly in resonance with the $^7F_6$–$^5D_4$ (20,533 cm^{-1}) transitions of Tb^{3+} ions in the host of Y_2O_3. Under 488 nm excitation, phonon-assisted transitions of $^7F_6$–$^5D_4$ happen. The phonon density, $\langle n \rangle = 1/e^{\hbar\omega/k_B T} - 1$, depends strongly on temperature. Here $\hbar\omega$ presents phonon energy, k_B the Boltzmann's constant and T the absolute temperature. As the temperature is elevated, $\langle n \rangle$ increases quickly. This will lead the phonon-assisted excitation of $^7F_6$–$^5D_4$ to increase; as a consequence, the intensity of the $^5D_4$–^7F_J transitions increases. In addition, there are different Stark splitting levels for the ground state $^7F_6$ and the excited state $^5D_4$. The electron population on each Stark level of $^7F_6$ depends on the temperature obeying the Boltzmann distribution. The higher the temperature, the larger the population of the upper level. The electron transition rate between different Stark levels of $^7F_6$–$^5D_4$ may be different, causing the $^7F_6$–$^5D_4$ excitation transitions to increase with temperature also. On the other hand, the thermal quenching effect of photoluminescence becomes strong as the temperature increases, leading the emission intensity of $^5D_4$–^7F_J to decrease. The two processes, photon-assisted excitation and the thermal quenching process both contribute to the intensity variation and rival each other. As the former process is dominant, the emission intensity increases. As the later process

surpasses the former one, the emission intensity decreases. Considering the two processes, the intensity as a function of temperature should appear a maximum at a certain temperature.

In Fig. 4, only one intensity maximum appears in the bulk, while two maximums appear in the NCs. This can be attributed to the existence of different Eu^{3+} centers in NCs. In Y_2O_3:Eu^{3+} NCs prepared by the same technique, two different luminescent centers, the internal and the surface, were identified by frequency-selective excitation spectra [20]. In the Y_2O_3:Tb^{3+} NCs, there should also exist two different luminescent centers, the internal and the surface. The number of surface Tb^{3+} centers increases largely with the decreasing particle size. In the bulk, the internal luminescent centers are dominant. It is suggested that the thermal quenching rates of the emissions between the surface and the interior Tb^{3+} ions are different. As is known, like concentration quenching, thermal quenching is induced by energy transfer from luminescent centers to defect levels [22]. In the surface, the Tb^{3+} ions near the involved surface defects act as quenching centers and do not contribute to the luminescence at all. Due to the random distribution of surface defects/ interior defects, a part of the surface Tb^{3+} ions are not close to the surface defects and they still act as luminescent centers. We suggest that since the energy transfer from surface luminescent Tb^{3+} ions to defects is hindered by the particle boundary [21], the thermal quenching rate of the surface luminescent Tb^{3+} centers decreases in comparison to that in the interior. As a result, the thermal quenching temperature increases. In $LaPO_4$: Eu^{3+}, we also determined that the thermal quenching rate in NCs decreased than that in the bulk [23]. It should be noted that, at present, we cannot exclude the possibility of valence state change between Tb^{3+} and Tb^{4+} in NCs with the increasing temperature.

4. Conclusions

The luminescent properties of cubic Y_2O_3:Tb^{3+} NCs (7–70 nm) prepared by combustion were studied under 488 nm excitation. The $^5D_4$–^7F_J ($J = 3-6$) emission lines for Tb^{3+} and a broad band around 620 nm caused by defects were observed. The emission intensity of the $^5D_4$–^7F_J transitions was proportional to the reverse of the particle size, while that of the defect levels linearly increased with particle size. Under 488 nm excitation, two intensity maximums for the $^5D_4$–^7F_J transitions of Tb^{3+} ions are observed in Y_2O_3:Tb^{3+} NCs, at ~250 and ~500 K, respectively, while only one maximum at ~250 K is observed in the bulk. Moreover, the relative intensity of the maximum at ~500 K to that at ~250 K increased with decreasing particle size. The appearance of intensity maximum of the $^5D_4$–^7F_J transitions was attributed to the rivalry between the phonon-assisted excitation of $^7F_6$–$^5D_4$ and the thermal quenching process. The former process leads the intensity to increase, while the later leads the intensity to decrease. The appearance of two maximums in the NCs was attributed to the luminescence of different Tb^{3+} centers, the internal and the surface. The photoluminescence for surface Tb^{3+} centers has relative high quenching temperature. In conclusion, the temperature-dependent luminescence behavior of Tb^{3+} in Y_2O_3:Tb^{3+} NC shows considerable difference in comparison to that in the bulk.

Acknowledgements

This work was finically supported by Nation Natural Science Foundation of China (Grant no. 10374083) and Talent Youth Foundation of Ji-Lin Province (Grant no. 20040105).

References

[1] A. Trave, F. Buda, A. Fasolino, Phys. Rev. Lett. 77 (1996) 5405.
[2] J.R. Agger, M.W. Anderson, M.E. Pemble, O. Terasaki, Y. Nozue, J. Phys. Chem. B 102 (1998) 3345.
[3] R.N. Bhargava, D. Gallagher, X. Hong, A. Nurmikko, Phys. Rev. Lett. 72 (1994) 416.
[4] S.B. Qadra, E.F. Skelton, D. Hsu, A.D. Dinsmore, J. Yang, H.F. Gray, B.R. Ratna, Phys. Rev. B 60 (1999) 9194.
[5] J. Yu, H. Liu, Y. Wang, F.E. Fernandez, W. Jia, L. Sun, C. Jin, D. Li, J. Liu, S. Huang, Opt. Lett. 22 (1997) 913.
[6] M. Ihara, T. Igarashi, T. Kusunoki, K. Ohno, J. Electrochem. Soc. 149 (2002) H72.

[7] K. Riwotzki, M. Haase, J. Phys. Chem. B 102 (1998) 916.
[8] M. Yada, M. Mihara, S. Mouri, T. Kijima, Adv. Mater. 14 (2002) 309.
[9] R.S. Meltzer, S.P. Feofilov, B. Tissue, Phys. Rev. B 60 (1999) R14012.
[10] H. Meyssamy, K. Riwotzki, A. Kornowski, S. Naused, M. Haase, Adv. Mater. 11 (1999) 840.
[11] H. Song, B. Chen, H. Peng, J. Zhang, Appl. Phys. Lett. 81 (2002) 1776.
[12] T. Igrashi, M. Ihara, T. Kusunoki, K. Ohno, Appl. Phys. Lett. 76 (2000) 1549.
[13] J. Wang, H. Song, B. Sun, X. Ren, B. Chen, W. Xu, Chem. Phys. Lett. 379 (507) (2003) 2003.
[14] D. Matsuura, Appl. Phys. Lett. 81 (2002) 4526.
[15] F. Vetrone, J.C. Boyer, J.A. Capobianco, A. Speghini, M. Bettinelli, J. Phys. Chem. B 107 (2003) 1107.
[16] H. Peng, H. Song, B. Chen, J. Wang, S. Lu, X. Kong, J. Chem. Phys. 118 (2003) 3277.
[17] H. Song, J. Wang, B. Chen, S. Lu, Chem. Phys. Lett. 376 (2003) 1.
[18] H. Song, B. Chen, B. Sun, J. Zhang, S. Lu, Chem. Phys. Lett. 372 (2003) 368.
[19] Y. Tao, G. Zhao, W. Zhang, S. Xia, Mater. Res. Bull. 32 (1997) 501.
[20] H. Peng, H. Song, B. Chen, J. Wang, S. Lu, J. Zhang, Chem. Phys. Lett. 370 (2003) 485.
[21] J. Wang, H. Song, B. Sun, X. Ren, B. Chen, W. Xu, Chem. Phys. Lett. 379 (2003) 507.
[22] Zhang, P. Xie, C. Duan, K. Yan, M. Yin, L. Lou, S. Xia, J.C. Krupa, Chem. Phys. Lett. 102 (1998) 10129.
[23] L. Yu, H. Song, S. Lu, Z. Lu, L. Yang, T. Wang, X. Kong, Mater. Res. Bull. 39 (2004) 2083.